NTNU – Trondheim
Norwegian University of
Science and Technology

CFD Study of Fuel-air Mixing in a Novel Low-NO_x Burner

Severin Reiz

August 2015

PROJECT REPORT

Department of Energy and Process Engineering

Norwegian University of Science and Technology

Supervisor 1: Professor Terese Løvås

Supervisor 2: Marcin Damian Dutka, MSc

Supervisor 3: Mario Ditaranto, PhD

Preface

This work has been carried as part of an internship in the Department of Energy and Process Engineering at NTNU during the spring semester of 2015.

It is assumed that the background of the reader of this report is related to science. The theory is explained in a separate chapter and readers that are familiar to fluid mechanics may skip this section.

Trondheim, 2015-08-01

Severin Reiz

Acknowledgment

Firstly, I would like to thank Dr. Mario Ditaranto and Prof. Terese Løvås for enabling international students to gain insights into current research topics at NTNU by this internship program. The cooperation with SINTEF is appreciated. Secondly, a project like this requires much assistance. I would like to thank Marcin Dutka for the great help in the setup of the numerical simulation and the continuous feedback. Suggestions and support by Mario and Terese are also gratefully acknowledged.

S.R.

Summary and Conclusions

The mixing between fuel and air in a combustion system is an important design parameter in accomplishing low NO_x emission performance. In an experimental study at NTNU a bluff body burner has been optimized by various parameters for optimal emission concentrations. Computational fluid dynamics (CFD) tools enhance this analysis as it provides additional data on the flow field. Nevertheless, a continuous verification of the simulation through experiment measurements is necessary in order to produce reliable results.

In the present work a CFD simulation of the experimental test rig has been carried out using RANS turbulence models. In a first step, the simulation is restricted to air flow only. Results are compared to experimental measurements. It was found that absolute values of velocities between experiment and simulation differ noticeable; relative trends, however, show similar flow behavior. This result was expected as literature reports poor performance of RANS turbulence models for this type of flow. Additionally, the pressure drop across the burner and mixing effects with ambient air are analyzed for different Reynolds numbers.

In a second step, fuel streams were added to the simulation. The concept of turbulent Schmidt numbers is used to model the mass mixing process and values suggested by Akbari [1] are assumed. Simulations are performed for methane and hydrogen as fuel. Fuel concentrations are recorded at different planes downstream of the burner lance. Fuel/air mixing prior to combustion is vital for low pollutant formation rates. In order to estimate a level of mixing the air/fuel equivalence ratio has been analyzed at a region before the fuel enters the flame. Results show good mixing properties but nevertheless several peaks of fuel concentrations appear.

Experimental measurements are collected from a small-scale test rig; in application much bigger power outputs are required. For this reason the issue of upscaling towards bigger burner geometries are investigated using the constraint of constant flow velocity. A simulation of a scaled burner geometry is conducted and results show that kinematic similarity is not applicable. An outlook towards more accurate results including a reactive flow simulation is given.

Contents

Chapter 1

Introduction

1.1 Motivation

Around the world countries face the transition to a more sustainable and renewable energy system. Nowadays, up to 80% of the world's energy consumption comes from fossil fuel combustion resulting in great amounts of human caused greenhouse gas emissions. Considering that combustion will continue to play a considerable role in future energy systems, one possible solution is the approach of "CO_2 capture and storage", often referred to as CCS. One such technology termed "pre-combustion capture" is based on decarbonizing the fuel and using hydrogen as fuel. The international research center BIGCCS combines academic and industrial institutions in the development of CCS energy solutions. Its target is to accelerate the development and use of large-scale CCS by basic research in the fields of CO_2 capture, transport and storage [3, 7].

However, CO_2 emissions are not the only concern in combustion systems; nitrogen oxides (NO_x) concentrations are a common side product of combustions and they are known to be harmful to humans. NO_x pollutant formation is a highly coupled phenomenon of chemical interactions and the flow field. Many studies focus on premixed combustion systems; partially premixed burners, however, show advantages regarding safety aspects. The level of mixing between fuel and air is an important design parameter and NO_x formation rates can be significantly reduced by an optimization of the air/fuel mixing [8].

BIGCCS is involved in a project at NTNU regarding hydrogen(H_2) combustion. The high reactivity and combustion temperature of H_2 are however challenging properties for the design

of low NOx burners. In an experimental test rig the influence of various factors on a partially premixed, bluff body stabilized burner have been investigated and results showed good performances in terms of emissions.

1.2 Background

The combustion characteristics of the developed burner is significantly influenced by the flow around the bluff body. The experimental measurements dominate the research development but certain information is very difficult to be measured in the experiment. Computational Fluid Dynamics (CFD) offers a great way of analyzing the flow field and can be an additional help in the understanding of the prevailing phenomena.

For this matter, a previous internship student at NTNU has performed a CFD study of the burner setup and investigated the computational performance of different turbulence models. The analysis was very similar to the procedure suggested by Dovizio performing a RANS simulation for a bluff body burner [5]. However, there occurred a few difficulties in the modeling approach of the previous study and thus, the model (e.g. Meshing) had to be re-done. Nevertheless, the previous study was helpful and improves the validity of the results as additional reference.

The task of the computational simulation started therefore from sketch with a drawing of the novel low NO_x burner. For operating conditions setting similar to experimental measurements were used.

1.3 Objectives

The scope of this project is to establish a CFD simulation of the burner. Firstly, for validity reasons the simulation requires a small comparison regarding the domain size and a mesh sensitivity study. Secondly, calculations with different turbulence models are performed and compared to PIV measurements of the experiments. In a third step, the mixing level prior to combustion is analyzed. Lastly, the burner design is upscaled towards industry required power throughputs. An outlook regarding a reactive flow analysis is given.

1.4 Limitations

In this study RANS turbulence models have been used. It is well known in literature that these models perform poorly for flow separation. However, it simplified the calculations and indicates a clear trend. Additionally, one should keep in mind that the flow field is largely affected by temperature/combustion in case of reactive flow. When evaluating the results one should be aware of these effects.

Chapter 2

Theory

In this chapter theoretical equations for modeling a turbulent fluid flow including species mixing processes are described. Furthermore, discretization methods for these equations are stated and the use in commercial software is explained.

2.1 Viscous flow analysis

2.1.1 Reynolds Averaged Navier-Stokes Equations

The physicist Navier and Stokes came up with a set of equations that describes the motion of fluids. Its derivation involves the conservation of mass, momentum and energy. There exist various forms of the equations depending on the application simplifications (e.g. Non-viscous/Viscous, Incompressible/Compressible). In general, the solution of the set of equations is a flow velocity.

For turbulence modeling an important bundle of methods uses the so called Reynolds Averaging. This means that the solution variables are decomposed into a mean component and a fluctuating one, e.g. $u_i = \bar{u}_i + u'_i$. By substituting this assumption in the respective equations one obtains the Reynolds-averaged Navier-Stokes (RANS) equations. In an Cartesian coordinate frame they can be written as

$$\frac{\partial \rho}{\partial t} + \frac{\partial}{\partial x_i}(\rho u_i) = 0 \tag{2.1}$$

$$\frac{\partial}{\partial t}(\rho u_i) + \frac{\partial}{\partial x_j}(\rho u_i u_j) = -\frac{\partial p}{\partial x_i} + \frac{\partial}{\partial x_j}[\mu(\frac{\partial u_i}{\partial x_i} + \frac{\partial u_j}{\partial x_i} - \frac{2}{3}\delta_{ij}\frac{\partial u_l}{\partial x_l})] + \frac{\partial}{\partial x_j}(-\rho\overline{u'_i u'_j}) \tag{2.2}$$

The term for the Reynolds stresses $-\rho\overline{u_i' u_j'}$ is responsible for the turbulence. Hence, one needs to use additional equations to model this term and to close the set of equations. A few different methods are described in the following section [2].

2.1.2 Turbulence Models

Standard k-ϵ Model

The k-ϵ model is the most popular turbulence model in the CFD world. The model consists of two separate transport equations that allows the calculation of a turbulent length and time scale. The first equation models the turbulent kinetic energy k, the second one its rate of dissipation ϵ.

$$\frac{\partial}{\partial t}(\rho k) + \frac{\partial}{\partial x_i}(\rho k u_i) = \frac{\partial}{\partial x_j}[(\mu - \frac{\mu_t}{\sigma_k})\frac{\partial k}{\partial x_j}] + G_k + G_b - \rho\epsilon - Y_M + S_k \tag{2.3}$$

$$\frac{\partial}{\partial t}(\rho\epsilon) + \frac{\partial}{\partial x_i}(\rho\epsilon u_i) = \frac{\partial}{\partial x_j}[(\mu + \frac{\mu_t}{\sigma_\epsilon})\frac{\partial \epsilon}{\partial x_j}] + C_{1\epsilon}\frac{\epsilon}{k}(G_k + C_{3\epsilon}G_b) - C_{2\epsilon}\rho\frac{\epsilon^2}{k} + S_\epsilon \tag{2.4}$$

Here, G_k is the generation of turbulence kinetic energy due to the mean velocity gradients and G_b represents the generation due to buoyancy. Y_m describes the contribution of the fluctuating dilatation in compressible turbulence to the overall dissipation rate. $C_{1\epsilon}$, $C_{2\epsilon}$ and $C_{3\epsilon}$ are constants and it is advisable at the beginning to use the default values that are determined by experimental measurements of air and water. σ_k and σ_ϵ denote the turbulent Prandtl numbers for k and ϵ respectively. S_k and S_ϵ represent user-defined source terms. The turbulent viscosity μ_t from equation 2.4 is computed by

$$\mu_t = \rho C_\mu \frac{k^2}{\epsilon}$$

where C_μ is a constant.

The vast popularity of the $k-\epsilon$ model can be explained by its robustness, economy and reasonable accuracy for a wide range of flow types. For flow separation, however, the model shows significant weaknesses. Modifications of the Standard k-ϵ model, such as RNG k-ϵ or realizable k-ϵ model, show improvements in the performance at certain conditions. In detail, the realizable $k-\epsilon$ model for example contains an alternative formulation for the turbulent viscosity and a modified transport equation for the dissipation rate ϵ [2].

Shear-Stress Transport (SST) $k-\omega$ Model

The SST $k-\omega$ model mixes the advantages of the regular $k-\omega$ formulation in near-wall regions and the $k-\epsilon$ model in the far field. A conversion from the regular $k-\epsilon$ version to a $k-\omega$ formulation is necessary.

The equation consequentially is an addition of the near-wall treatment k-ω and the far field formulation transformed k-ϵ – each multiplied with a blending function and one minus the blending function, respectively. Close to the wall the blending function is defined as one - hence the advantages of the $k-\omega$ model prevail. In the far field the blending function approaches zero and the transformed $k-\epsilon$ model dominates.

The formulation of the SST k-ω model have a similar form as in the Standard k-ω model:

$$\frac{\partial}{\partial t}(\rho k) + \frac{\partial}{\partial x_i}(\rho k u_i) = \frac{\partial}{\partial x_j}(\Gamma_k \frac{\partial k}{\partial x_j}) + G_k - Y_k + S_k \tag{2.5}$$

$$\frac{\partial}{\partial t}(\rho \omega) + \frac{\partial}{\partial x_j}(\rho \omega u_j) = \frac{\partial}{\partial x_j}(\Gamma_\omega \frac{\partial \omega}{\partial x_j}) + G_\omega - Y\omega + D_\omega + S_\omega \tag{2.6}$$

G_k denotes the generation of turbulence kinetic energy k and G_ω the generation of ω. Γ_k and Γ_ω represent the effective diffusivity, Y_k and Y_ω the dissipation of k and ω, respectively. D_ω is a cross diffusion term. S_k and S_ω are user-defined source terms [2].

2.1.3 Species Transport Equations

The local mass fraction of each species is described by the convection-diffusion equation. It reads in the general form

$$\frac{\partial}{\partial t}(\rho Y_i) + \nabla(\rho \bar{v} Y_i) = -\nabla \bar{J}_i + R_i + S_i \tag{2.7}$$

where R_i represents the rate of production of species i by chemical reaction, S_i the rate of production by a dispersed phase or any user-defined sources. These equations will be solved for N-1 species where N is the number of species involved. The last species is solved by the fact that mass fractions sum up to one.

In turbulent flows, mass diffusion is computed in the following form:

$$\bar{J}_i = -(\rho D_{i,m} + \frac{\mu_t}{Sc_t})\nabla Y_i - D_{T,i}\frac{\nabla T}{T} \tag{2.8}$$

where Sc_t represents the turbulent Schmidt number($\frac{\mu_t}{\rho D_t}$ where μ_t denotes the turbulent viscosity and D_t the turbulent diffusivity).

2.2 Numerical treatment

2.2.1 Discretization Methods

In a mathematically sense, the upper described sets of equations are a non-linear type of partial differential equations. Mathematicians still struggle proving the existence and the smoothness of the solution. Nevertheless, engineers use them widely without concerns and the solutions are very useful and beneficial in flow analysis. For computational fluid dynamics a discretization is almost always the first cornerstone.

The continuous domain is divided into discretized cells (mesh) and a control-volume based technique is used to convert the transport equations from above to an algebraic form that can be solved numerically. Depending on the discretization method this results in different forms of coupled equations. Scalar quantities are transported within neighboring cells and depending on the mesh topology and the complexity of the equations this results in a coefficient matrix. Most CFD codes use the "Finite volume method".

Note that regarding the method divergence may occur when the intermediate flow field varies to largely from the solution. One may start the calculation with first order methods and switch to second order methods to remove numerical errors(dissipation).

A common approach in CFD for solving the equation system is a pressure-based solution method. First it solves for the velocities components in the flow field, then it applies a pressure correction (continuity), updates the flow field and lastly, it solves the other equations (e.g. energy, species and turbulence). As soon as the residual (loosely speaking, the error) ranges within a given convergence threshold, the calculation is terminated [2].

2.2.2 Commercial CFD Software

The present study focuses on applying CFD in order to investigate a flow field and not to go into the development of efficient CFD codes. There exists various published CFD software and for many applications they are more economical and reliable than self-written code. An overview of available open-source and commercial CFD codes can be found on the CFD-online website [4].

The software ANSYS Fluent allows the simulation of all ranges of fluid flow, turbulence, heat transfer and chemical reactions. Fluent is integrated in the ANSYS workbench module which allows users to create the geometry in the corresponding ANSYS DesignModeler and to generate the mesh in the ANSYS Meshing tool. In the Fluent module the case is set up by specifying the materials, boundary conditions and solution methods. Fluent uses the “Finite Volume Method" where the user defines the desired discretization order. The solution method can be selected as segregated or coupled; for scalar equations the system is solved by a point implicit Gauss-Seidel scheme in conjunction with an algebraic multigrid (AMG) method [2].

Chapter 3

Methodology

In the following chapter the basic methodology of the CFD simulation is described. In a first step a simulation of air-flow only is conducted. A mesh sensitivity study is obtained and the calculations are compared to PIV measurements. In a second step fuel streams are injected. An upscaled model was investigated regarding similarity measures. Post-processing steps are explained, such as how the equivalence ratio at the location where the flow enters the flame is analyzed. An outlook for a reactive flow simulation is given.

3.1 Specification of the fluid domain

3.1.1 Description of the experimental setup

The investigated in-house bluff body stabilized burner consists of a stainless steel conical bluff body with diameter d = 28 mm, concentrically fitted within a pipe of diameter D = 34mm. The pipe is formed convergent with a final diameter of 25mm (see figure 3.1) and serves as air inlet. There are eight primary fuel inlets of $2.0mm$ equally distributed around the circumference at $17.3mm$ from the apex of the cone. Four secondary fuel inlets of $1.4mm$ are located at $4.7mm$ from the top of the cone. The rate of mass flow through the primary or secondary fuel inlet can be adjusted. For the test conditions of the CFD simulation the burner is exposed to atmosphere.

The burner lance is shifted upstream (X3 in figure 3.1) such that a gap of $1mm$ between the

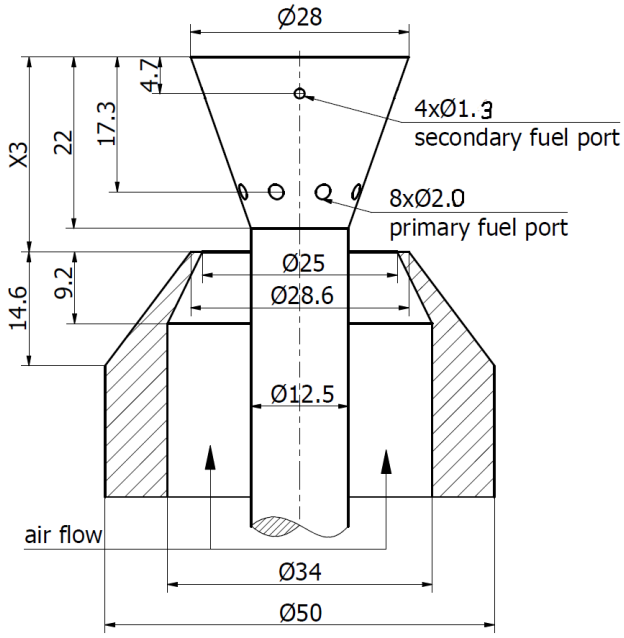

Figure 3.1: Burner specifications

lance and the case remains. This X3 distance was experimentally investigated by a parameter variation and this value showed good performance regarding emissions. Recall also, that this is a partial premixed burner (fuel and air are separated upstream) which has advantages regarding safety aspects. Flame propagation upstream of the fuel ports is impossible. The flow around the bluff body stabilizes the flame position. Good mixing properties, however, are required for low NOx emissions.

3.1.2 Computational domain

The geometry is rotational symmetric by 90° due to the secondary fuel ports. Hence, only a quarter of the domain has been analyzed. The following assumptions are made:

- Air Flow: duct length ca.5 times its thickness to develop turbulent velocity profile
- Fuel Inlets: Duct lengths at least 3 times diameter to develop turbulent velocity profile
- Cut section: Periodic Boundary Condition on respective faces of quarterly cut geometry
- Burner exposed to environment: Pressure outlet at fictive boundaries

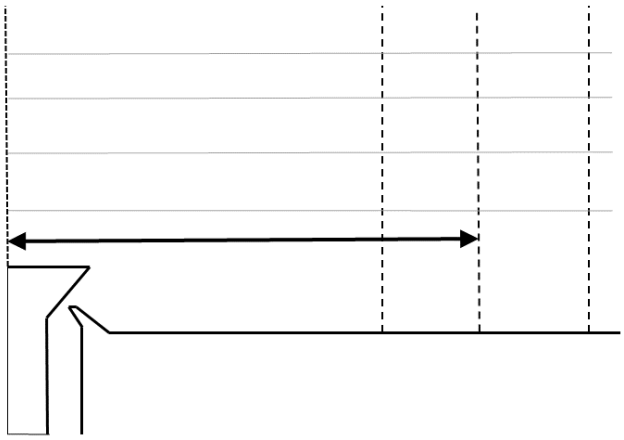

Figure 3.2: Different domain sizes including locations of comparison

The last point raises further questions. The burner is exposed to environment but a computational domain must be delimited. A fixed domain length of $20cm$ downstream was used as this corresponds to the position of the lance used for emission measurements in the experiment. Nevertheless, the width of the simulation domain was not specified. For this cause, a short analysis regarding the domain size was made. The geometry was enlarged and the velocity profiles are compared at different locations downstream. Figure 3.2 explains this procedure.

Cases for a geometry chamber of diameter of $105mm$, $150mm$ and $200mm$ are calculated. The Mesh is equivalent for the inner body and cells are only added to the outside of the cylinder. The axial velocity is plotted for different locations downstream in figure 3.3. The plot for $10mm$ downstream 3.3a shows equivalent profiles. At the location of $20mm$ downstream(3.3b) velocity differences in the chamber center for the domain of $105mm$ occur. In plot 3.3c and 3.3d the difference between $105mm$ and the others can also be noticed. $150mm$ and $200mm$ domain show almost equivalent profiles in all plots. Consequentially, a domain enlargement further than $150mm$ does not influence the flow field. In order to keep the amount of elements as low as possible the domain size of diameter $150mm$ is used onwards.

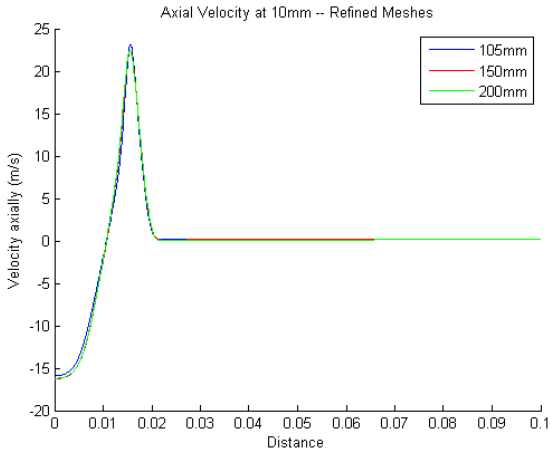

(a) 10mm

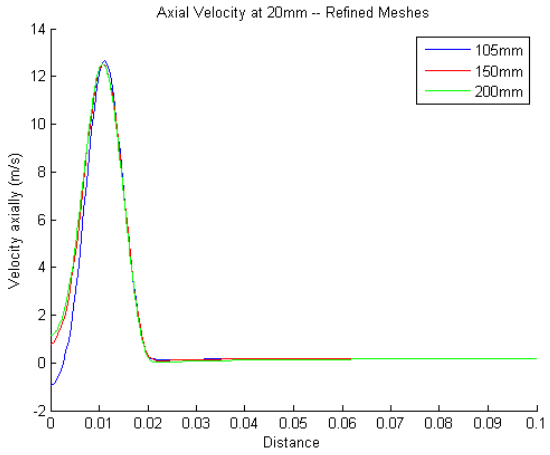

(b) 20mm

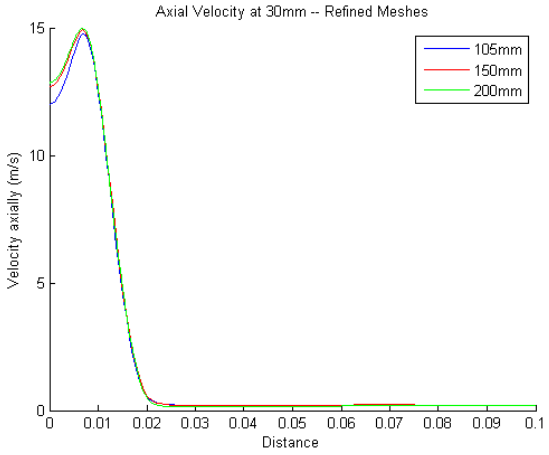

(c) 30mm

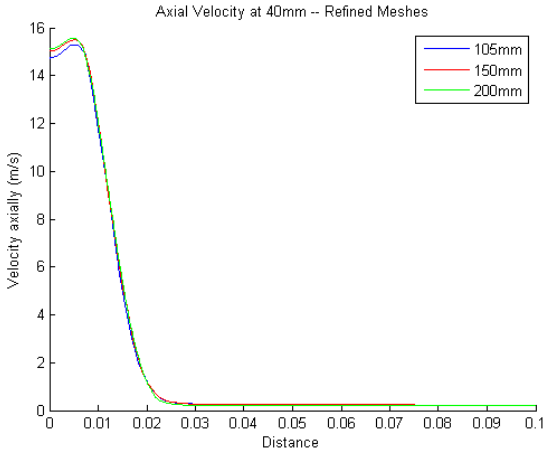

(d) 40mm

Figure 3.3: Comparison of domain sizes - Plot axial velocity along radial distance at different locations downstream

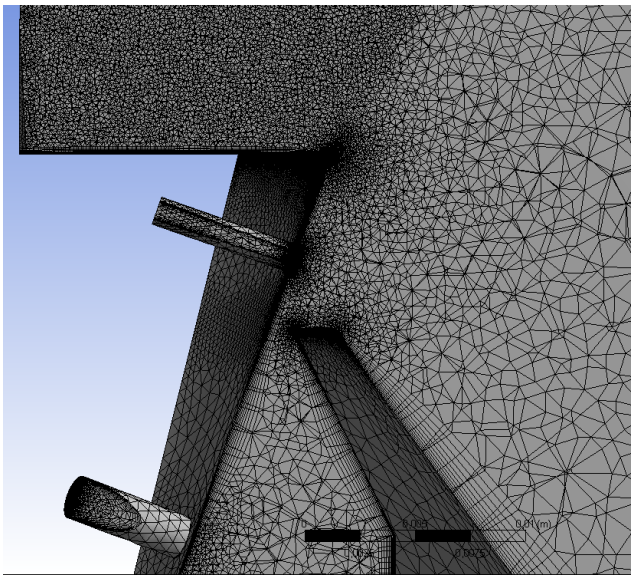

Figure 3.4: Tetrahedral mesh cells in cross section of secondary fuel port

3.2 Mesh Generation

3.2.1 Meshing features

The previous student used a regular hexahedral mesh which has disadvantages for inclined edges/surfaces. Tetrahedral elements overcome these problems as they can adapt to various geometry types; however, they are more complicated to use and usually more cells are required. Nevertheless, a tetrahedral mesh was generated in *Ansys Meshing* using the settings listed in table A.1. A mesh sensitivity study was obtained using these meshes. In general, mesh refinements are placed at:

- Flow separation zone
- Gap between lance and case
- Fuel inlets

An inflation layer is added at faces where a boundary layer develops; due to the periodic boundary conditions the mesh on the cut surfaces is equivalent. The periodic boundary conditions links these surfaces and by using the same discretization on the respective surfaces, no intermediate interpolation during the calculation is necessary.

Figure 3.4 shows the mesh in a section plane at the location of the secondary fuel port. One can observe the upper mentioned refinement zones and the inflation layers.

3.2.2 Mesh sensitivity study

For validity reasons a mesh sensitivity study was performed. The test case is an ordinary air-flow only calculation. Velocity profiles along the upper mentioned lines downstream are plotted. One can see equivalent profiles of the velocity at the analyzed locations. Therefore, Mesh 1 with the smallest number of elements has been used onwards.

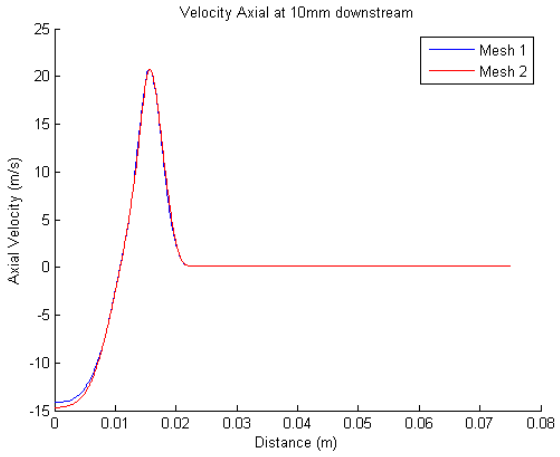

(a) 10mm

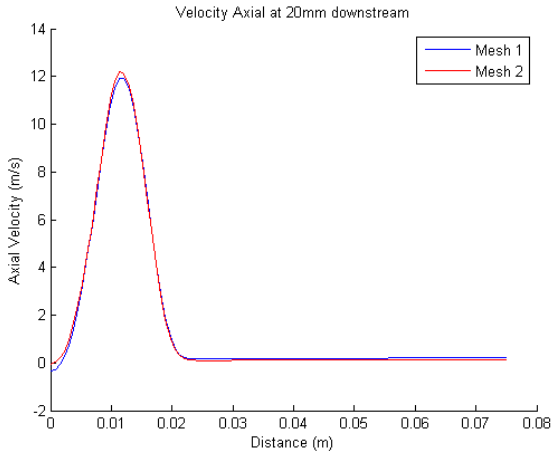

(b) 20mm

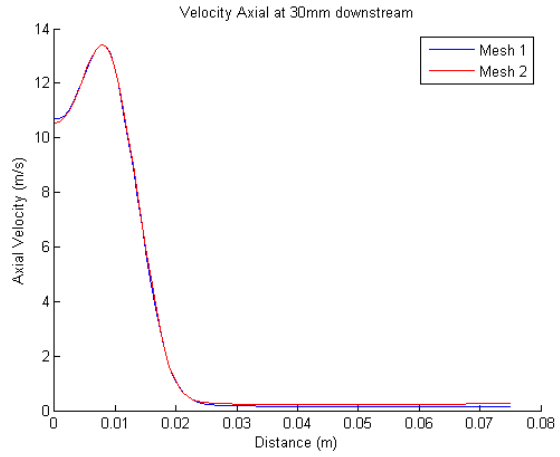

(c) 30mm

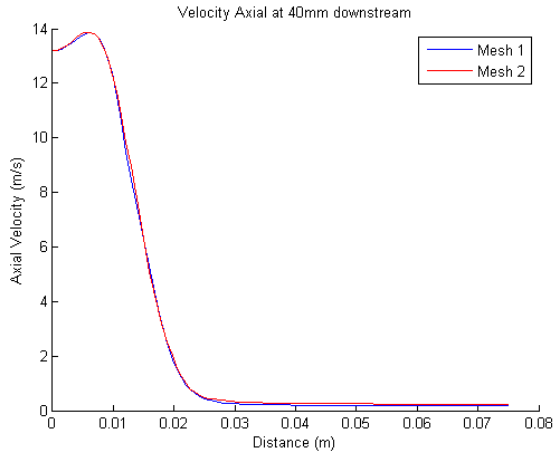

(d) 40mm

Figure 3.5: Mesh sensitivity study - Plot axial velocity along radial distance at different locations downstream

3.3 Test conditions

Mass flow inlets have been used for the respective inlets and a pressure outlet was assumed at faces exposed to the environment. For walls a non-slip boundary condition was specified.

At first, a simulation of only air flow was calculated. 2 different mass flow rates were investigated that are specified in table A.2. Results where compared to experimental data measured by PIV.

In a second step, fuel streams were added to the flow. Mass flow rates similar to an experimental case are used and tabulated in table A.4 and A.5. A turbulent species mixing process requires the specification of a turbulent Schmidt number. Akbari [1] had investigated this influence in a similar setup. He suggests suitable Sc_t numbers for Hydrogen and Methane mass mixing and besides, he mentions the poor performance of RANS modules. Nevertheless, the suggested values of $Sc_t = 0.7$ for Methane and $Sc_t = 0.4$ for Hydrogen are used.

Addtionally, the pressure drop was investigated for different Reynolds numbers. Settings are described in the appendix.

3.4 Upscaling

As a constraint it has been assumed that flow velocities should be kept constant. For this reason the flow area is increased to achieve a higher mass flow and power generation.

The burner design is round and the cross-sectional area at any location can be described by

$$A_{cross} = \pi * (r_{outer}^2 - r_{inner}^2)$$

where r_{outer} is the outer radius of the flow area "ring" and r_{inner} the inner radius.

In order to increase power production rates by a factor C, assuming constant flow velocity the area needs to be scaled by the Upscaling factor.

$$A_{cross} = C * \pi * (r_{outer}^2 - r_{inner}^2) = \pi * [(\sqrt{C} * r_{outer})^2 - (\sqrt{C} * r_{inner})^2]$$

Hence, the lab scale geometry dimensions need to be scaled by a factor of $\sqrt{C}$.

In this particular case the lab burner is operated at $10kW$. The desired upscaled burner should run at $200kW$. Consequentially the burner throughput is scaled by a factor of 20 and hence, all geometry dimensions by $\sqrt{20}$.

3.5 Calculation procedure

Since the generated meshes are fairly big, calculations consume a considerable amount of computational effort. Therefore, the Kongull Cluster by the NTNU HPC group has been used. Kongull is a Linux cluster running Rocks and contains 113 nodes with 1 login, 4 I/O and 108 compute nodes. In most cases the Dell Xeon based nodes were used that cosist of two Intel Xeon CPU E5-2670 @ 2.60 GHz 8-core (SandyBridge) processors. Details can be found on the website of the Kongull cluster [6]. The calculation job was then passed through a batch scheduling system, OpenMPI and the Fluent module started on the nodes. A sample jobscript can also be found on the Kongull website. Fast calculations were found with at most 1 core per 100k Cells, so usually about 2 nodes with 8 processors per node were used.

For the convergence a good practice was the SIMPLEC method with an adapted Underrelaxation factor in pressure to 0.7. Additionally, the following procedure was tested to be reliable: First order methods in all equations until residuals are fairly low, then switch to second order methods in all equations but the pressure until (almost) convergence and finally use second order methods in all equations to remove numerical dissipation. The initialization with a previous converged calculation and a close look into the residuals are worthwhile. The default convergence limit of 1e-3 is often not sufficient and a reduction to 1e-5 was necessary.

3.6 Post-processing the results

3.6.1 Air flow only

Velocity analysis

The post-processing steps of the CFD results has been done in *CFDpost*. As mentioned already in figure 3.2 horizontal lines downstream of the bluff body are analyzed. These locations are

$10mm$, $20mm$, $30mm$ and $40mm$ behind the top of the lance. The recirculation zone downstream of the bluff body is of great importance which ends less than $25mm$ behind the burner apex in all calculations and measurements. Hence, the velocity profiles up to $40mm$ cover the interesting flow phenomena. These velocities are compared with PIV measurements. The Reynolds number was calculated through

$$Re = \frac{\rho * D * v}{\mu}$$

where the diameter of the bluff body was used as characteristic length D and v is assumed to be the average velocity in the burner throat.

Pressure drop

Furthermore, the pressure drop was investigated for different Reynolds numbers. The pressure coefficient is calculated through

$$c_p = \frac{\textbf{static pressure}}{\textbf{dynamic pressure}} = \frac{p_2 - p_1}{0.5 * \rho * v^2}$$

For the pressure drop across the whole burner p_2 is located at the inlet of the burner and p_1 at the pressure outlet. p_1 is zero in the simulation due to the assumed pressure boundary condition. Note that due to the location of p_2 the inlet velocity is used for v (contrary to Reynolds number calculation). In many scenarios the Euler number is more convenient than c_p. It is defined as

$$Eu = \frac{c_p}{2}$$

.

Ambient air entrainment

Another investigated phenomenon dealt with the question, how much ambient air is mixed in the flow prior to the flame. In the simulation the burner is exposed to the environment and air is "sucked" in by the stream. This effect influences the fuel concentrations in the combustion. Velocity vectors in figure 3.6 demonstrate this phenomenon and a surface is added at a suitable

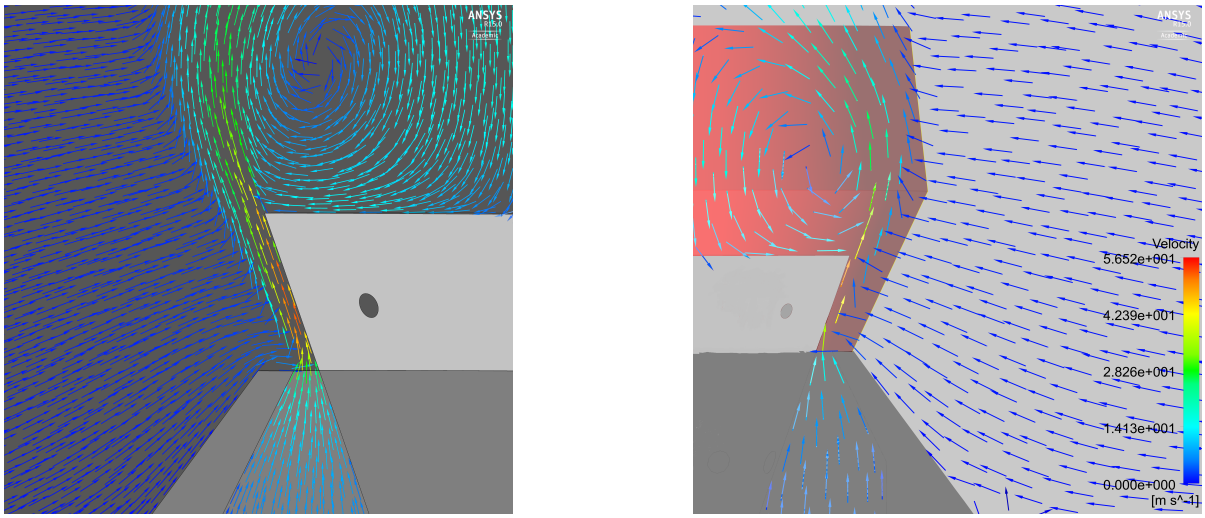

(a) Flow field showing the entrainment of ambient air in the flow

(b) Fictive surface(red) to measure ambient air mass flow involved in entrainment

Figure 3.6: Ambient air entrainment

location. Mass flow across this surface is analyzed and compared to the inlet mass flow. The surface ends at the stagnation point of the respective case.

3.6.2 Mass diffusion

For the mixture fractions planes at the aforementioned locations are created and the mixture fractions are plotted in contour plots. As an outlook a “flame surface" has been created for a mixture analysis. Since the flow field is largely affected by temperature/combustion in case of reactive flow, this approach is very inaccurate. The flame is located in the shear layer of the recirculation zone. The fictive surface is then an iso-clip surface where the velocity equals 3m/s and $Y > 0.0m$ (behind lance) and radial distance $< 1.5cm$. The flame specifications results from the fact that the recirculation zone slows down the flow and due to volumetric expansion the recirculation zone is moved slightly downstream.

For the value of the equivalence ratio an additional variable was created in CFD post.

Definition of equivalence ratio

The Fuel-air equivalence ratio (Φ) is defined as

$$\Phi = \frac{\textbf{fuel-to-oxidizer ratio}}{(\textbf{fuel-to-oxidizer ratio})_{st}}$$

Methane-air combustion

The investigated case involves the following stoichiometric balanced chemical reaction

$$CH_4 + 2O_2 \rightarrow CO_2 + 2H_2O$$

Therefore, the Fuel equivalence ratio reads

$$\Phi = \frac{m_{CH_4}/m_{O_2}}{(m_{CH_4}/m_{O_2})_{st}}$$

Hence, one needs to examine the stoichiometric conditions, i.e.

$$(m_{CH_4}/m_{O_2})_{st} = \frac{1*(12+4)}{2*(2*16)} = \frac{1}{4}$$

The equivalence ratio Φ can converted to be based on air mixture (assuming a molar percentage $\chi_{O_2} = 0.2094$ of oxygen).

$$\Phi = \frac{m_{CH_4}/m_{O_2}}{(m_{CH_4}/m_{O_2})_{st}} = 4*m_{CH_4}/m_{O_2} = 4*m_{CH_4}/(\chi_{O_2}*m_{air}) = \frac{4}{\chi_{O_2}} * \frac{m_{CH_4}}{m_{total}} * \frac{m_{total}}{m_{air}}$$

The last expression uses molar fractions only and has been used for the calculations.

Hydrogen-air combustion

In this case the chemical reaction reads

$$2H_2 + O_2 \rightarrow H_2O$$

The stoichiometric conditions result in

$$(m_{H_2}/m_{O_2})_{st} = \frac{2*(2*1)}{(2*16)} = \frac{2}{16} = \frac{1}{8}$$

Using the aforementioned result, the equivalence ratio Φ is obtained as

$$\Phi = \frac{m_{H_2}/m_{O_2}}{(m_{CH_4}/m_{O_2})_{st}} = \frac{8}{\chi_{O_2}} * \frac{m_{H_2}}{m_{total}} * \frac{m_{total}}{m_{air}}$$

Again, the last expression which involves only mass fraction is used for postprocessing the CFD results.

Chapter 4

Results

4.1 Air Flow only

As general overview figure 4.1 shows a streamline plot of the flow around the bluff body in the burner. The recirculation zone plays a major role in the burner because the flame is located in the shear layer. Flow velocity in the shear layer is reduced and the position quite stable over time. Hence, a stabilized flame will be formed at this location. However, one should keep in mind that the recirculation zone is increased significantly due to volumetric expansion in the reactive case.

4.1.1 Recirculation zone

Due to the upper mentioned flame position the recirculation zone is of main interest in the simulation. In the course of the experimental study PIV measurements are collected at the test site. This data is compared to the simulation regarding the recirculation zone length and width.

Recirculation zone length

Axial velocities in the the wake of the bluff body are plotted in figure 4.2. The relative velocity profile shows a similar behavior compared to the experiments. However, one can see significant differences between absolute velocities. The simulation using the $k-\omega$ model shows better performance than $k-\epsilon$ in terms of recirculation length. Absolute value of the results from the

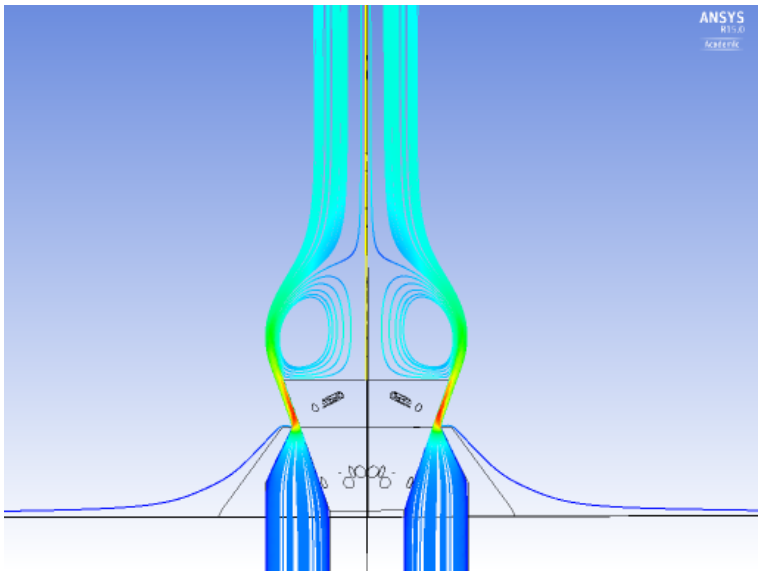

Figure 4.1: Streamline plot - air flow only

$k-\epsilon$ model range closer to experimental measurements. Note that in this investigated test case an average velocity of $32 m/s$ is measured in the gap between lance and case, i.e. smallest cross-section.

Recirculation zone width

Among the length of the recirculation also the width of the recirculation zone is of interest. For a better comparison the radial position of the vortex center is analyzed instead which has a great correlation with the recirculation width. Results are tabulated below. Note that the listed velocities in the table correspond to the average velocities in the gap. Due to the fact that the resolution of the experimental PIV measurements is roughly $1 mm$ one can conclude good agreement between experiment and simulation. Furthermore, experimental measurements showed that the radial vortex center position remains unchanged for changed conditions. The simulation shows a small correction towards the experimental value.

Table 4.1: Radial position of vortex center

	32m/s	16m/s
Simulation $k-\epsilon$	11.40 mm	11.03 mm
Simulation $k-\omega$	11.02 mm	—
Experiment	10.04 mm	10.04 mm

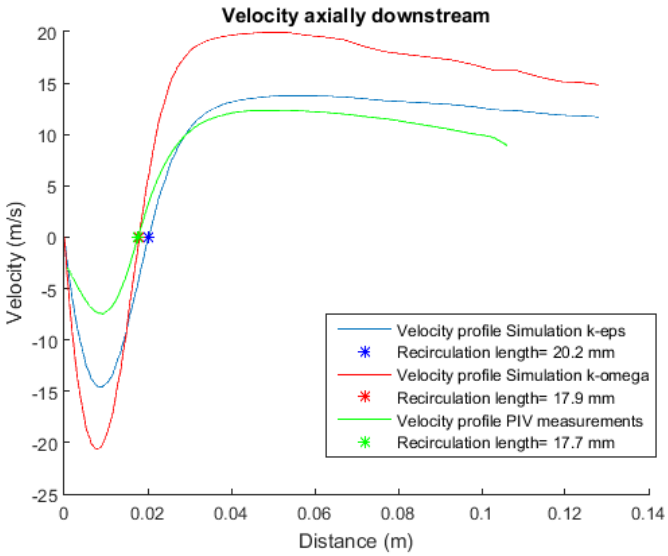

Figure 4.2: Axial velocity along central axis downstream behind lance apex for Re=57 300

4.1.2 Pressure drop

The pressure drop corresponds to the energy that needs to be provided to maintain the flow velocity. At the outlet a pressure of 0 Pa is assumed and hence the pressure drop is driven by the inlet pressure. Pressure drop in the burner corresponds to the Euler number, as described in section 3.6.1. Plot 4.3 shows the Euler number for different Reynolds numbers. The observed qualitative behavior is typical for a flow around a bluff body. Following the theory of self similar flow the pressure drop decreases for a higher Reynolds numbers up to the critical point. Then, the flow is fully turbulent and the pressure drop remains constant for higher velocities.

However, it is remarkable that absolute values are particularly high. The small gap of 1 mm between lance and case results in fast velocities but also requires an increased pressure drop.

4.1.3 Mixing with ambient air

This section deals with the question of how much ambient air is "sucked" in by the flow. This kind of mass mixing decreases the equivalence ratio and, loosely speaking, reduces the temperature and thermal NO_x pollutant formation. It is interesting to see how much contribution is made by this side-effect.

Table 4.2 lists the ratio of ambient air mass flow rate to inlet mass flow rate. Indeed, a consid-

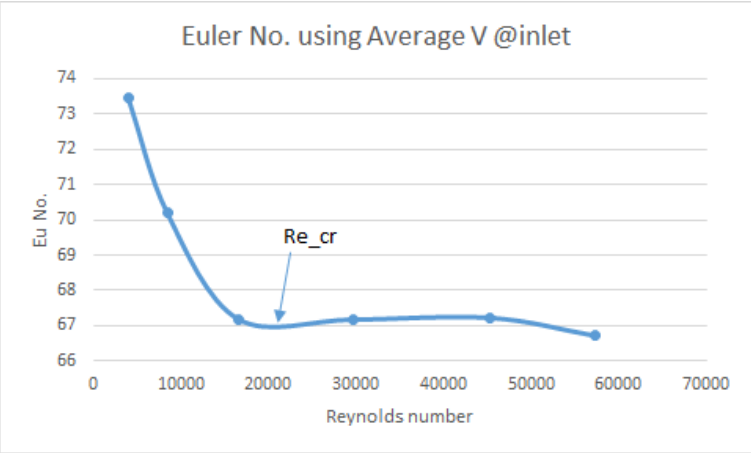

Figure 4.3: Euler numbers for different Reynolds numbers

Table 4.2: Ambient air mixing for different Reynolds numbers

Re number	$\dot{m}_{ambient}/\dot{m}_{inlet}$
57 300	1.46
29 600	1.357
16 570	0.618
9 500	0.597

erable amount of ambient air is mixed with the flow. The intuitive behavior regarding different flow velocities is confirmed. For higher flow velocities not only more ambient air is mixed but also the dimensionless ratio is increased. Consequentially, one cannot neglect ambient air mixing in a fuel concentration analysis.

4.2 Mass Mixing

In the following fuel streams have been added to the simulation. Good mixing between fuel and air prior to combustion is necessary to achieve low NOx conditions. A clear distinction between Methane and Hydrogen is made because species mixing processes are highly dependent on the material parameters.

4.2.1 Methane-Air

Fuel concentrations at several planes downstream are displayed in figure 4.4. In subplot 4.6a one can see clear peaks of fuel concentration at locations of fuel inlets. This peaks gradually

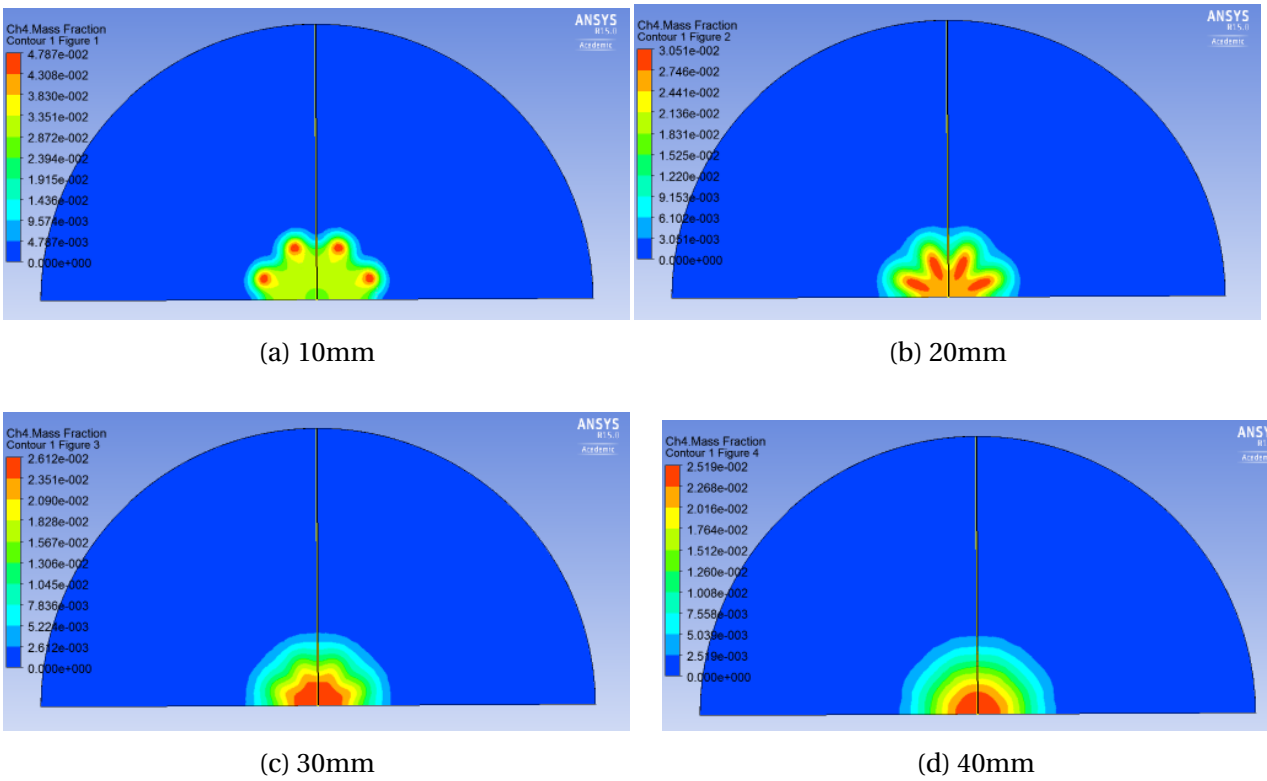

(a) 10mm (b) 20mm

(c) 30mm (d) 40mm

Figure 4.4: Contour plot of methane fuel concentrations at several locations downstream

fade out for measurement points further downstream. This corresponds to the intuitive mass mixing process. At the location of $40mm$ behind the apex of the lance the fuel concentration is equally distributed at radial distances. Furthermore, fuel mixing may be enhanced by secondary fuel ports which have been inactive at this stage.

Additionally, the equivalence ratio was analyzed on a fictive flame surface in figure 4.5. One can see the variations of fuel concentrations due to the position of the fuel inlets. High equivalence ratios occur at the lance's edge where flow separation develops. Furthermore, the average value of the equivalence ratio for that respective surface is 0.599. Ambient air is mixed with the fuel/air-stream from inside the duct.

4.2.2 Hydrogen-Air

The burner can be used for different fuel compositions. Due to different material properties mixing processes need to be distinguished regarding fuel species.

In figure 4.7 the equivalence ratio is plotted on the fictive flame surface. One can see peaks

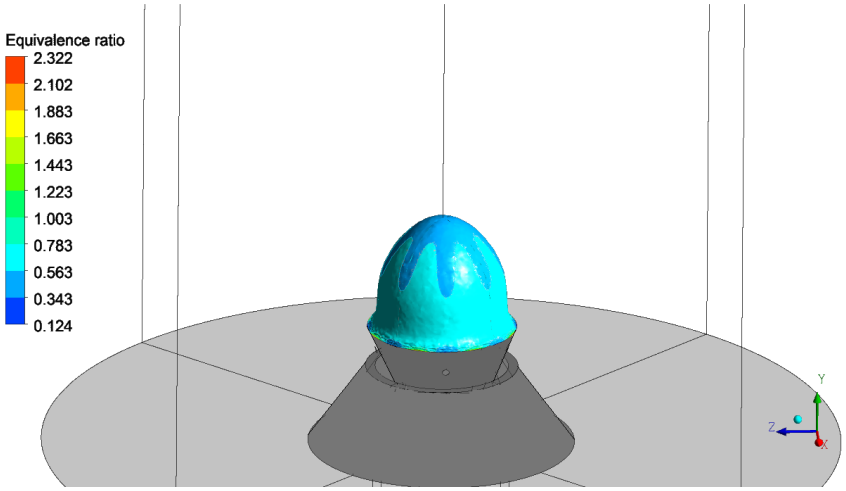

Figure 4.5: Contour plot of equivalence ratio on fictive Methane flame surface

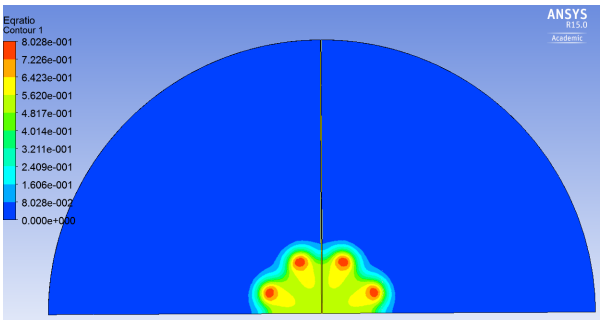

(a) 10mm

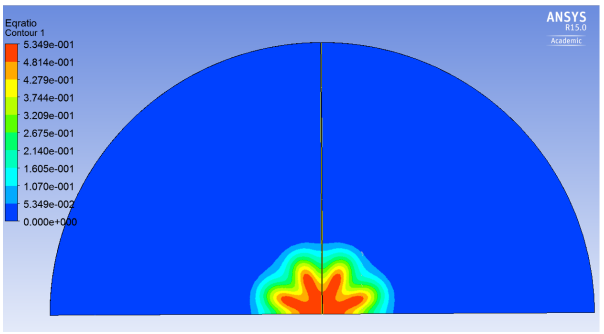

(b) 20mm

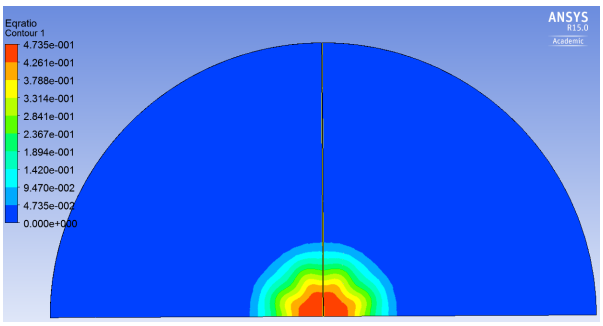

(c) 30mm

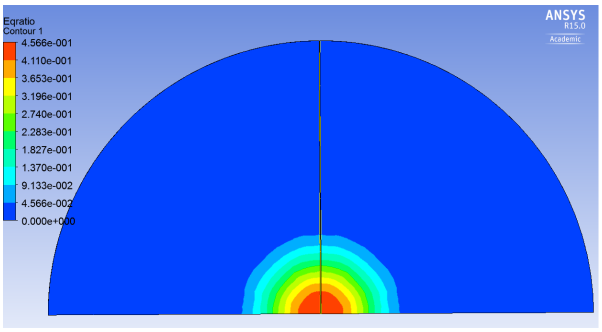

(d) 40mm

Figure 4.6: Contour plot of fuel concentrations of Hydrogen at several locations downstream

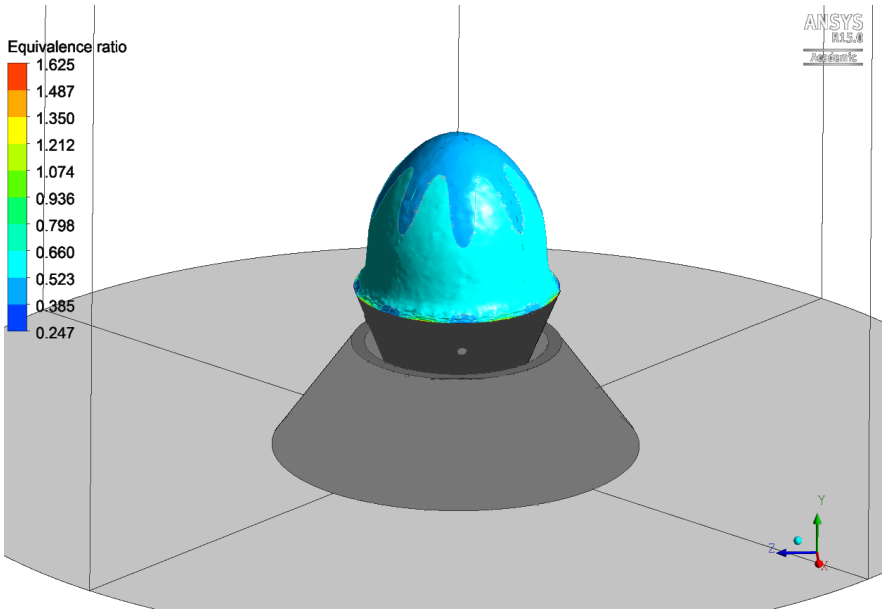

Figure 4.7: Contour plot of equivalence ratio on fictive Hydrogen flame surface

up to 1.625 are obtained at the lance of the burner. The average equivalence ratio is 0.547.

4.3 Upscaling

Geometric similarity requires physical lengths to be similar to the prototype model; this is guaranteed as the whole model is scaled by a constant factor. To achieve the greater power output one needs to multiply the mass flow rate by the desired enlargement factor; consequentially velocities equivalent to the lab burner are expected.

Kinematic similarity describes the similarity in terms of time and flow motion. This refers to the streamline paths as well as to the velocity distributions. At the air flow inlet similarity is given as cross-sectional area and mass flow rate is increased by the same factor.

4.3.1 Similarity in the recirculation zone

Upscaling of the geometry with unchanged material parameters and the constraint of constant velocity results in an increased Reynolds number. The lab scale Reynolds number is approxi-

Table 4.3: Kinematic Similarity

	Lab Scale model	Upscaled model
Recirculation length/diameter$_{bluff\ body}$	0.617	0.467
Recirculation width/diameter$_{bluff\ body}$	0.405	0.394

mately multiplied by the respective upscaling factor.

$$Re = \frac{\rho * v * D_{upscaled}}{\mu} = \frac{\rho * v * (D_{lab} * C)}{\mu} = 221680 \simeq C * Re_{lab}$$

Note that the velocity in the gap used for Reynolds calculation is reduced slightly in the upscaled model. In terms of absolute values, the lab scale simulation calculates an average velocity of approx. 32 m/s, the scaled simulation a velocity of 27.6 m/s. This is suprising since a constant velocity has been used as a constraint for Upscaling. Residuums in the scaled case are below the limit of $1e-5$ using second order methods, so convergence should be obtained and numerical errors sufficiently small. Nevertheless, the upscaled case is analyzed regarding flow similarity in the following. Note that Reynolds numbers are much bigger in the upscaled case, so a complete similar result is not expected.

Dimensionless features of the recirculation zone are listed in table 4.3. One can observe that the dimensionless recirculation length is shorter in the upscaled model. In other words, this means that the recirculation length is not increased by the same factor as the geometry dimensions. This effect can be explained by unchanged material parameters and therefore no given Reynolds similarity.

Interestingly, the dimensionless recirculation width remains nearly constant. This effect has also been reported from experimental measurements. Increasing velocities (i.e. Reynolds numbers) produce almost the same recirculation width.

4.3.2 Comparison of pressure drops

Figure 4.8 shows the Euler number for the upscaled simulation plotted together with the lab-scale results. Although the Reynolds number is a lot higher in the upscaled case, an Euler number close to the previous simulations is expected. However, the upscaled case shows a remarkable low Euler number is obtained. Consequentially, the theory of the self similar flow and the

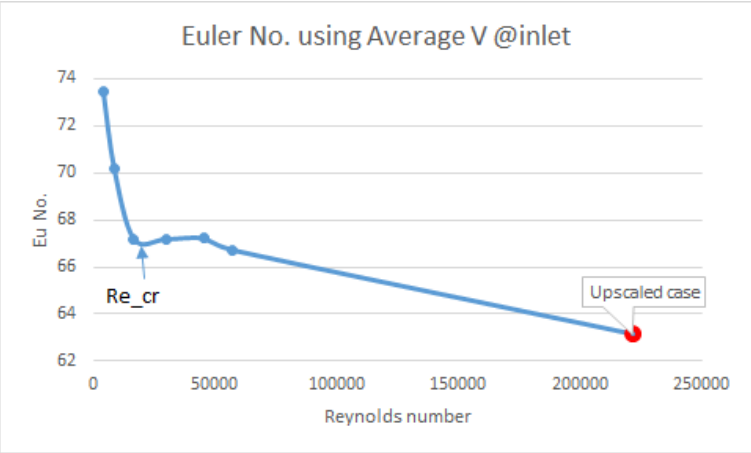

Figure 4.8: Euler number for upscaled geometry

piecewise constant pressure drop is not applicable for this naive upscaling approach.

Chapter 5

Summary and Recommendations for Further Work

5.1 Summary and Conclusions

In an experimental test rig at NTNU an in-house bluff body stabilized burner is investigated regarding emission concentrations, showing good performances in terms of emissions and stability at 10 kW. A CFD simulation was created for the experimental burner geometry using a dense tetrahedral mesh and 1/4 of the geometry exploiting symmetry. Since the test rig is open to environment a short study on the necessary computational domain was made. This study revealed that a chamber-formed domain of diameter=150 mm is sufficient assuming a pressure-outlet boundary conditions on the surfaces exposed to environment. A mesh sensitivity study proved that the element sizing is acceptable.

Simulations using this mesh are performed for different RANS turbulence models, i.e. $k-\epsilon$ Standard, $k-\epsilon$ Realizable and $k-\omega$ model. The results are compared to PIV measurements and noticeable differences between simulation and experiment data occurred. This result was nevertheless expected since RANS turbulence models' performance is weak for flows including flow separation zones. A simulation using different turbulence approaches, e.g. LES, was not performed due to high computational complexity and the emphasis on the analysis of fuel mixing processes. However, relative trends of the simulation results showed similar behavior as the experiment; the $k-\epsilon$ Standard showed the closest correspondence to experiment and was used

for the next tasks.

Mass flow rates in the burner were adjusted to investigate different flow regimes. On the one hand, the pressure drop across the burner was decreasing for higher Reynolds numbers until a critical point of Re=20 000; above that critical Reynolds number the flow becomes self similar and the pressure drop remains constant. On the other hand, the phenomenon of air entrainment was investigated. It was found that for a Re=57 300 1.46 times more ambient air is mixed in prospective flame regions than inlet injected air. This effect lowers fuel concentrations in the burner and changes combustion properties.

In a next step fuel streams are added to the flow; hydrogen and methane are treated separately due to different mixing properties. Turbulent Schmidt numbers suggested by Akbari are used [1]. Results showed expected and intuitive mixing effects. A reactive simulation influences mixing and the flow significantly due to volumetric expansion, etc. First tries on a reactive case are made, but many problems occurred as a 3D reactive simulation is not straightforward.

Lastly, the issue of upscaling flow phenomena towards greater power outputs was investigated using the approach of constant flow velocity. Results are compared to the lab-scale model regarding similarity features. The dimensionless recirculation length was decreased compared to the lab-scaled simulation, whereas the dimensionless recirculation width remained constant. The results about the recirculation width are not surprising; by its nature the recirculation width is driven by the diameter of the bluff body. In general, flow features are significantly influenced by upscaling. Furthermore, the pressure drop was decreased in the upscaled case compared to the lab scale. The theory of self similar flow is not applicable to naive upscaling as there may be non-linear factors involved.

5.2 Discussion

Due to geometry of the burner meshing strategies are not straightforward and considering having many skewed surfaces a tetrahedral mesh is advisable. Special treatment with small element sizes are required at the fuel ports, the burner throat and the separation zone. Another problematic region is the boundary layer. To enhance calculations in near wall-regions inflation layers are used at wall surfaces; however, in order to further decrease Y+ values the transition of el-

ement sizes needs to be very smooth (Growth ratio). Furthermore, increasing the number of inflation layers helps in achieving lower Y+ values.

The fact that RANS turbulence models perform poorly for flows involving flow separation, as literature reports, is confirmed. Nevertheless, since relative flow behavior is simulated well the use is justified. However, to obtain more accurate results the choice of the turbulence model needs to be reconsidered.

CFD results showed a remarkably high pressure drop across the burner. A flow gap of 1 mm in the burner throat is advantageous for low pollutant concentrations; but this also bears the disadvantage of a comparably high pressure drop across the burner. Low pressure drops are preferred in industry due to less compression work.

Regarding fuel concentration prediction results show that the effect of air entrainment can not be neglected. Ambient air is mixed in flame regions which changes the combustion reactant distribution. The experimental setup is slightly different when emission measurements are collected; a chamber is placed around the burner to prohibit exhaust gas mixing with the environment. For this case one should also consider that hot exhaust gas may be mixed with the flow through an additional, outer recirculation zone. In experiment, lower NO_x emission concentrations are measured for a small gap in the burner throat, resulting in higher velocities. It is difficult to find reasons for this behavior. One approach may be that this is also caused by a greater influence of the air entrainment effect for higher velocities.

The issue of upscaling has been addressed using a constant velocity approach. Since the dimensionless recirculation length shows a significant reduction, it can be assumed that kinematic similarity is not applicable. This result shows that predicting the flow field for bigger geometries is not straightforward. In order to evaluate the scaled geometry a reactive simulation would be helpful. Upscaling the flow characteristics responsible for pollutant formation mechanisms will be necessary.

5.3 Recommendations for Further Work

The simulation shows a few weaknesses as described in the section 5.2. First, some words on the turbulence model need to be said. It is well known that RANS turbulence models perform

poor for flows involving flow separation. Despite of that fact they have been used because they are easy to handle, robust and very economical. Nevertheless, one can enhance the simulation by using a more complex description to model the turbulence terms. However, steps towards e.g. a Large-Eddy simulation are not straightforward and will consume a lot of modeling and computational effort.

Secondly, the simulation needs to be extended for a reactive case. The flow field is significantly influenced by adding a flame due to volumetric expansion, exhaust gas diffusion etc. A few tries have been made using a pdf composition and the GRI 3.0 mechanism but this naive approach did not lead to an ignited flame. Nevertheless, it is recommended to simulate the reactive case first, and then moving to a more complicated turbulence model.

A long term goal will be reactive simulation that can be upscaled to greater power ranges. Experiments with big power outputs are expensive and here, an upscaled numerical simulation will be very helpful; necessary upscaled solutions could be provided. The key idea is to reproduce flow characteristics responsible for pollutant formation in greater power ranges.

Appendix A

Additional Information

A.1 Methodology

A.1.1 Meshing Settings

The Meshing is performed in *Ansys Meshing* using the lower listed settings. Match Control is responsible for equivalent meshes on cut surfaces (periodic boundary conditions). For this option a rotational Coordinate system and a symmetry plane needs to be defined in the geometry. The meshing algorithm for these faces is “Pre" and thus, it was not possible in the software to work with additional refinement levels. Consequentially, sizing constraints were added.

The default values have been used for the other parameters. For the inflation layers a number of 10 layers and a growth ratio of 1.1 was used in order to decrease the Y+ value. Mesh 3 was created but as mesh 1 and mesh 2 showed similar behavior it has not been used for calculations. Mesh 1 and mesh 2 are sufficiently small to cover all flow phenomena.

A.1.2 Test conditions

Air flow only

Since only a quarter of the domain was simulated the mass flow rate from the table A.2 must be divided by four. In an additional case a mass flow rate of $1.77116 kg/s$ was tested.

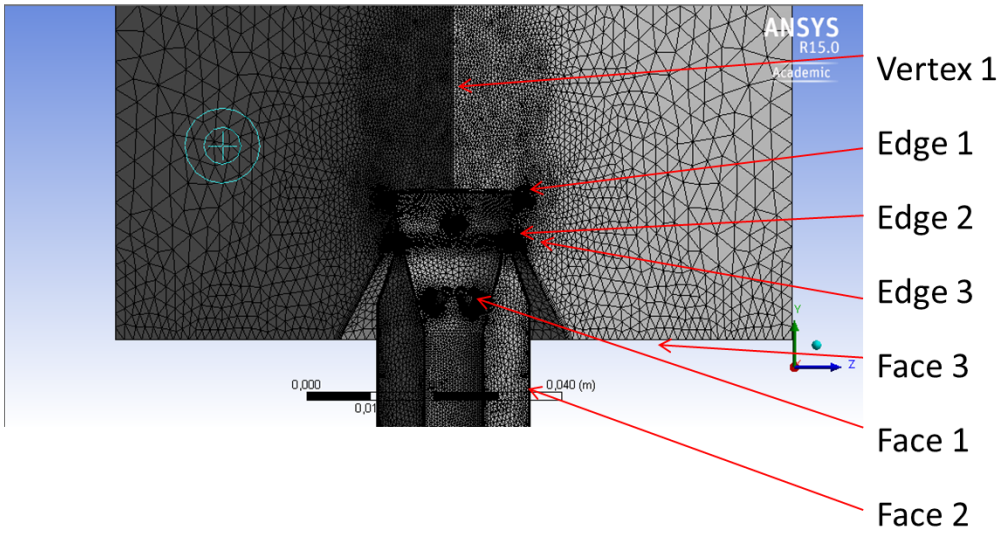

Figure A.1: Name Labeling for table A.1

Table A.1: Meshing Settings

	Mesh 1	Mesh 2	Mesh3
Inflation layers	Yes	Yes	Yes
Match Control	Yes	Yes	Yes
Sizing Edge1- end of lance	3e-5 m	3e-5 m	2e-5 m
Sizing Edge2 - case inner	2e-5 m	2e-5 m	1e-5 m
Sizing Edge3 - case outer	4e-5 m	4e-5 m	2e-5 m
Sizing Vertex1 (Sphere radius 1.9e-2m)	8e-4 m	3e-4 m	2.2e-4 m
Sizing Face1- Fuel Inlets and its edges	5e-6 m	5e-6 m	5e-6 m
Face2 - inside burner	5e-4 m	5e-4 m	5 e-4 m
Face 3 - outside to atmosphere	2e-3 m	2e-3 m	1e-3 m
Sizing Face4- Fuel Inlets	5e-5 m	5e-5 m	5e-5 m
Global cell size	1.8e-3 m	1.8e-3 m	1.8e-3 m
Cells	3.1 million	8.2 million	10 million

Table A.2: Settings for case of air flow only

Mass flow rate of air:	$3.80417071e-3 kg/s$
Density of air:	$1.204 kg/m^3$
Dynamic viscosity of air	1.846e-5 Pa*s
Turbulence intensity:	10%

Table A.3: Mass flow rates for different Reynolds numbers - air flow only

Air mass flow rate $\dot{m}$	Re
0.00025 kg/s	3 900
0.0005 kg/s	9 500
0.001 kg/s	16 600
0.001902 kg/s	29 600
0.00398041 kg/s	57 300

Table A.4: Settings for case of Air-Methane mass mixing

Mass flow rate of air:	3.9858e-3 kg/s
Methane mass flow rate:	1.99800e-4 kg/s

Test conditions pressure drop

Settings from table A.3 have been used for the parameter study of the pressure drop analysis. Since only a quarter of the domain was investigated these rates divided by four have been used in the Fluent settings. For Reynolds number smaller than 20 000 a laminar simulation was performed.

Settings for Fuel-Air mass diffusion

The same values for the air density, viscosity and the turbulence intensity are used. In these cases only primary fuel ports are used. In each fuel port an eighth of the specified mass flow rate occurs. Table A.4 lists the mass flows for the methane case where a turbulent Schmidt number was used. Table A.5 specifies the Hydrogen Case where $Sc_t = 0.4$ has been assumed.

A.1.3 Tricks for convergence

In order to start the calculations the data filed needs to be initialized. Fluent offers a initialization mechanism for doing so. The hybrid initialization with default parameters were found to be a good start for the iterations.

Table A.5: Settings for case of Air-Hydrogen mass mixing

Mass flow rate of air:	3.3069997e-3 kg/s
Hydrogen mass flow rate:	8.33333e-5 kg/s

Additionally, when one struggles with divergence the following tips can help to solve these problems:

1. Try to use previous case files as initialization. E.g.: Initialize $k-\omega$ Simulation with $k-\epsilon$, other Reynolds number with a previous case of other $\dot{m}$, Mass mixing with air flow only
2. Start with laminar settings and switch to turbulent once residuums are fairly small; Note: initializing laminar simulation with turbulent data file resulted always in divergence!
3. Use first order methods at the beginning for all equations
4. Switch to second order methods in all equations except pressure
5. At the end switch to second order methods in all equations

A.1.4 Description of files

The provided USB drive serves as a start for further simulations. For each investigated simulation the Fluent case file (.cas) and data file (.dat) is provided. The case file included the mesh topology and the case specifications, such as boundary conditions and solution methods. The corresponding data file is a solution file after a certain iterations, so that residua are below an acceptable threshold. In some cases the residua are stuck at a point and stopped decreasing; a phenomenon due to the steady assumption although the flow is changing over time (transient). For further investigations one can look at the residuum plots after reading the case and data file in Fluent. Furthermore, in case someone desires to modify a case, one may initialize the solution with the given data file. Note, that if the mesh is changed the case cannot be initialized with the given data file. One needs to initialize the case with the new mesh first. However, the case file can be used as a basis as Fluent offers the "Replace Mesh" functionality.

Post-processing steps have been made in CFDpost. For this reason state files of CFDpost for faster post-processing are provided. For plotting graphs .csv files are exported for a data series and imported into MATLAB.

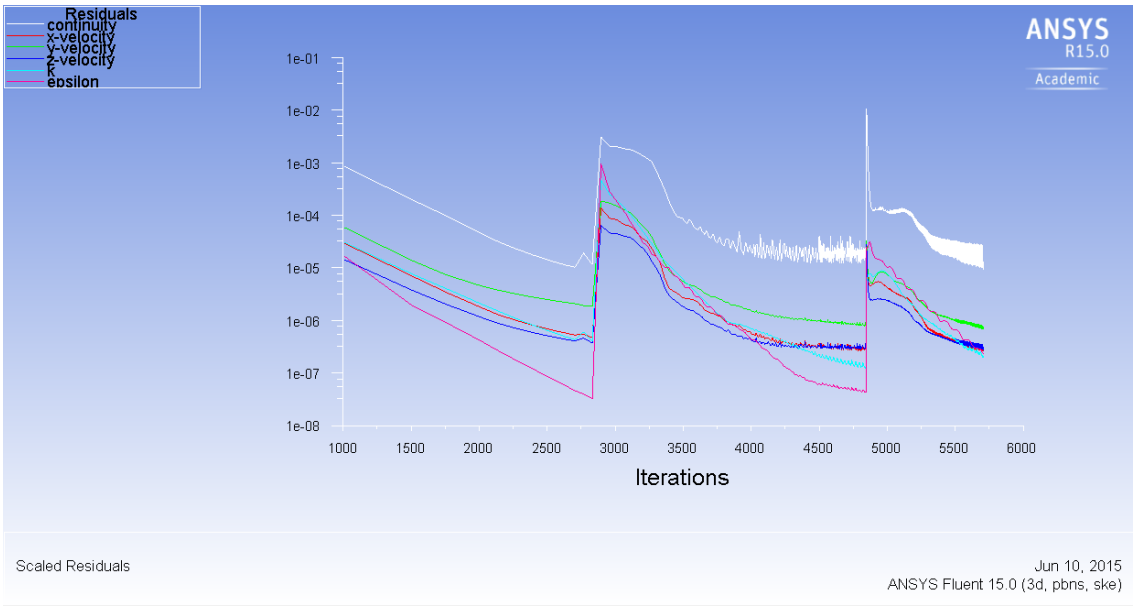

Figure A.2: Residual plot k-eps Air flow only, Re=57 300

A.2 Results

A.2.1 Residuums

In figure A.2 a sample residual plot is given. One can see a sawtooth behavior. The residual is decreased to a certain point, then discretization methods are switched to second order in all equations but pressure, and lastly the pressure discretization is also switched to second order. The oscillating behavior is also normal for this type of flow. One should stop the calculations when the oscillations show no general decreasing anymore.

A.2.2 Y-Plus values

The Y-Plus value is a dimensionless wall distance indicating the boundary layer. It is used as a quality measurement of the underlying mesh. Figure A.3 shows a contour plot of the Y-Plus value in a $k-\epsilon$ simulation. One can see that in the apex of the lance and behind the gap between lance and case peaks of the Y-Plus value up to 5.5 occur. One needs to be c

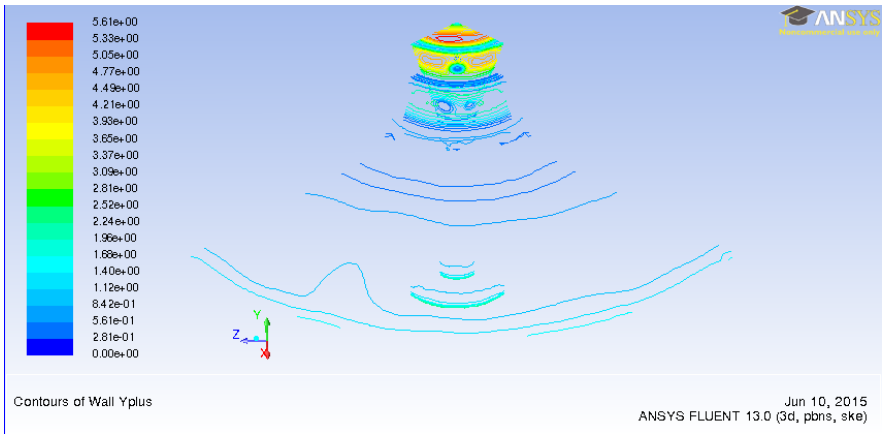

Figure A.3: Contour plot of Y-Plus values with k-eps model simulation air flow only, Re=57 300, Y+max=5.6

Bibliography

[1] A. Akbari, S. Hill, V. McDonell, and S. Samuelsen. Experimental and computational analyses of methane and hydrogen mixing in a model premixer. *Journal of Engineering for Gas Turbines and Power*, 133(10):101503, 2011.

[2] ANSYS, Inc. ANSYS Fluent Theory Guide, Nov. 2013. Release 15.0.

[3] BIGCCS International CCS Research Centre. Website, http://www.bigccs.no, July 2015.

[4] CFDonline. Website, http://www.cfd-online.com/wiki/codes. Website, July 2015.

[5] D. Dovizio, M. M. Salehi, and C. B. Devaud. Rans simulation of a turbulent premixed bluff body flame using conditional source-term estimation. *Combustion Theory and Modelling*, 17(5):935–959, 2013.

[6] HPC NTNU. http://www.hpc.ntnu.no/display/hpc/kongull. Website, July 2015.

[7] The World Bank. Database Fossil Fuel Energy Consumption. http://data.worldbank.org/, July 2015.

[8] J. Warnatz, U. Maas, and R. W. Dibble. *Combustion: Physical and Chemical Fundamentals, Modeling and Simulation, Experiments, Pollutant Formation.* Springer, 2006.